Check for updates

Exploring a new dinuclear Fe(III) complex for the fixation of atmospheric CO_2 and optical recognition of nano-molar levels of Zn^{2+} ions†

Seikh Taniya, Somnath Khanra, Sabyasachi Ta, Sudeshna Chatterjee, Noor Salam* and Debasis Das [ID] *

A dinuclear Fe(III) complex (**F1**) of an imine derivative (**L1**) derived from 3-ethoxy-2-hydroxy-benzaldehyde and hydrazine, structurally characterised *via* single crystal X-ray studies, is employed for the catalytic conversion of epoxides to cyclic carbonates utilizing carbon dioxide. In addition, **F1** is employed for the selective optical recognition of nano-molar levels of Zn^{2+} (42.23 nM) *via* a metal displacement approach. The Job plot reveals interactions between **F1** and Zn^{2+} at a 1 : 3 molar ratio with an association constant of 7.71×10^4 M^{-1}. Studies on the catecholase-like activity of **F1** reveal a k_{cat} value of 4.42×10^3 h^{-1}.

Introduction

Despite the high abundance of iron at the earth's surface, its bio-availability at physiological pH under aerobic conditions is low.[1,2] However, the role of iron in bio-systems is highly significant. For example, it is involved in energy transfer and bio-catalysis,[3] and acts as a cofactor of several enzymes.[4] Iron deficiency may cause liver dysfunction and anaemia, whereas its presence at higher concentrations may lead to hemochromatosis and Parkinson's disease.[5] It is well known that iron deficiency in pregnant women can adversely affect both the mother and infant, including an increased risk of sepsis, maternal mortality, perinatal mortality, and low birth weight.[6]

Similarly, Zn^{2+} plays a significant role in several biological processes,[7] including in brain activity, gene transcription, immune functioning, *etc.*[8,9] It is a cofactor of almost three hundred enzymes,[10] including those involved in DNA repair and gene expression.[11] On the other hand, abnormal zinc metabolism leads to several health issues, including delayed sexual maturation, prostate cancer, type 2 diabetes mellitus (T2DM), Wilson's disease, amyotrophic lateral sclerosis (ALS), and age-related macular degeneration (AMD).[12–14] It is believed that Zn^{2+} homeostasis has some correspondence with the pathology

of Alzheimer's disease[15] and other brutal neurological problems, such as cerebral ischemia[4] and epilepsy.[5]

Currently, the catalytic activities of metal complexes have acquired significant attention. Scientists are attempting to lower carbon dioxide levels[16–18] in the atmosphere through its conversion to cyclic carbonates using metal complexes as catalysts. The cyclo-addition of CO_2 and epoxides, forming cyclic carbonates, is a process with 100% atom economy[19–21] that can lead to reduced CO_2 levels. Moreover, cyclic carbonates have enormous numbers of industrial applications, for example as non-toxic/polar/high boiling solvents, electrolytes in lithium ion batteries, reactive intermediates, *etc.*[22] However, the low reactivity of CO_2 means that a catalyst[23–25] is required for the cyclo-addition reactions to be feasible. Iron compounds,[26] having low intrinsic toxicity, can catalyse the combination of CO_2 and epoxides to form cyclic carbonates.[27,28]

These facts motivated us to study the catalytic activity of a new iron complex for the fixation of CO_2 as cyclic carbonates using different epoxides.

Additionally, catechol oxidase of the oxidoreductase class of enzymes is very vital in biological systems.[29–34] The use of transition metal complexes as bio-catalysts that can mimic catechol oxidase has become a pioneering field of research.

Therefore, the above discussion clearly demonstrates our motivation for investigating the optical recognition[35–38] of the bio-relevant metal ion Zn(II) and the (bio)catalytic application of a new Fe(III) complex.

Herein, a new dinuclear Fe(III) complex (**F1**), structurally characterized *via* single crystal X-ray diffraction analysis, is used for the selective optical recognition of nanomolar levels of Zn^{2+}. **F1** functions as an excellent catalyst for the fixation of atmospheric CO_2 as cyclic carbonates using epoxides. Moreover, the catecholase-like activity of **F1** has been investigated. Finally, **F1**

Department of Chemistry, The University of Burdwan, Burdwan, 713104, W.B., India. E-mail: ddas100in@yahoo.com; Fax: +91-342-2530452; Tel: +91-342-2533913 ext. 424

is also established as a good extractor of Zn(II) from water to ethyl acetate.

## Experimental

Synthesis

N,N′-Bis-(2-hydroxo-3-ethoxy-benzylidene)-hydrazine (L1). 3-Ethoxy-2-hydroxy-benzaldehyde (166.17 mg, 1 mmol) was refluxed with a slight excess of hydrazine in methanol for 8 h to get **L1** in 91.5% yield. Its molecular formula is $C_{18}H_{20}N_2O_4$ (MW = 328.36 g mol^{-1}). Anal. found (%): C, 65.65; H, 6.20; and N, 8.02; calcd (%): C, 65.84; H, 6.14; and N, 8.53. ESI-MS (*m/z*): $[M]^+$, 327.75 (Fig. S1a, ESI†). ^{1}H NMR (CDCl$_3$, 400 MHz, *J*, Hz, *δ* ppm) (Fig. S1b, ESI†): 13.928 (1H, s) 8.234 (1H, s), 6.824–6.841 (1H, q) 6.783–6.761 (1H, q), 6.723–6.684 (1H, t, *J* = 7.8 Hz), 4.097–4.041 (2H, m), 3.304–3.280 (1H, q). FTIR (KBr, cm^{-1}): 3336, *ν*(O–H); 3196, *ν*(C–H, aromatic); 1684, *ν*(C=O, stretch); 1500, *ν*(C=N); 1068, *ν*(N–N) (Fig. S1c, ESI†).

Dinuclear Fe(III) complex (F1)

Methanol solution of FeCl$_3$·6H$_2$O (27 mg, 0.1 mmol, 5 mL) was added to DMF solution of **L1** (50 mg, 1.5 mmol, 5 mL), and the mixture was stirred for 2 h. The mixture was kept for a week for the growth of black crystals, which were suitable for SC-XRD analysis (Fig. 1a). The yield was 64%. Its molecular formula is $C_{54}H_{54}Fe_2N_2O_{12}$ (MW = 1090.73 g mol^{-1}). Anal. found (%): C, 59.41; H, 5.13; and N, 7.10; calcd (%): C, 59.46; H, 4.99; and N, 7.70. ESI-MS (*m/z*): $[M]^+$, 1113.08 (Fig. S2a, ESI†). FTIR (KBr, cm^{-1}): 3011, *ν*(C–H, aromatic); 1639, *ν*(C=O); 1451, *ν*(C=N); 1140, *ν*(N–N) (Fig. S2b, ESI†).

Zn(II) adduct (Z1)

Ethanol solution of **F1** was stirred with Zn(OAc)$_2$ and kept for 3 days to get the **Z1** adduct in 59% yield (Fig. 1b). Its molecular formula is $C_{20}H_{23}N_2O_5Zn$ (MW = 436.80 g mol^{-1}). Anal. found (%): C, 54.72; H, 5.40; and N, 6.04; calcd (%): C, 54.99; H, 5.31; and N, 6.41. ESI-MS (*m/z*): $[M]^+$, 435.50 (Fig. S3a, ESI†). FTIR (KBr, cm^{-1}): 3169, *ν*(C–H, aromatic); 165, *ν*(C=O); 1481, *ν*(C=N); 1227, *ν*(N–N) (Fig. S3b, ESI†) (Scheme 1).
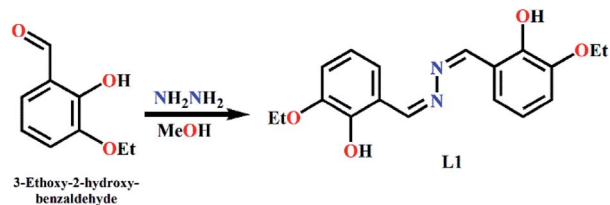
Scheme 1 The synthetic protocol for **L1**.

Results and discussion

The single crystal X-ray structure of F1 (ref. 39)

It is desirable to confirm the structure of a new compound *via* single crystal X-ray diffraction (SC-XRD) analysis. Thus, in addition to the spectroscopic characterization of **F1**, its structure is authenticated from SC-XRD analysis (Fig. 1a). The crystallographic data and refinement parameters are presented in Table S1 (ESI).† Selected bond lengths and angles are listed in Table S2 (ESI).† **F1** is triclinic, having the space group $P\bar{1}$ (CCDC 1864282), with *a* (Å): 14.8885(7); *b* (Å): 15.0825(6); *c* (Å): 15.1336(6); *α* (°): 104.859(3); *β* (°): 104.285(3); *γ* (°): 117.418(3); volume (Å^3): 2639.0(2); and *Z* = 2, and adopts octahedral geometry around both Fe(III) centres. **L1** exhibits *cis* geometry in the complex with selected bond lengths N1–C00P: 1.294(9) Å; and N2–C00U: 1.284(9) Å, indicating the presence of –CH=N double bonds. Bond angles of O004–Fe01–O007: 96.1(2)°; O004–Fe01–O003: 94.2(2)°; O003–Fe01–N3: 92.3(2)°; O004–Fe01–N00J: 83.9(2)°; O007–Fe01–N00J: 93.6(2)°; and N3–Fe01–N00J: 89.3(2)° clearly reveal the octahedral geometry around the Fe(III) centres. Symmetrical **L1** contributes to each of the Fe(III) centres unbiasedly and co-ordinates *via* phenol *O*- and aldimine *N*-groups, with Fe01–O003 and Fe01–N2 bond lengths of 1.920(4) Å and 2.197(6) Å, respectively.

Spectroscopic studies

The absorption characteristics of **F1** were studied using UV-vis spectroscopy. **F1** exhibits two significant absorption peaks at 296 nm and 358 nm, which can be assigned to π–π* and n–π* electronic transitions (Fig. 2a). Upon the gradual addition of
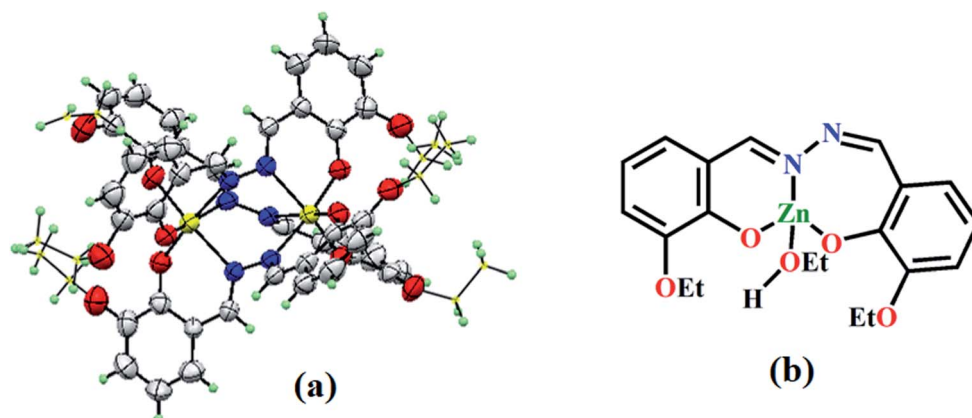
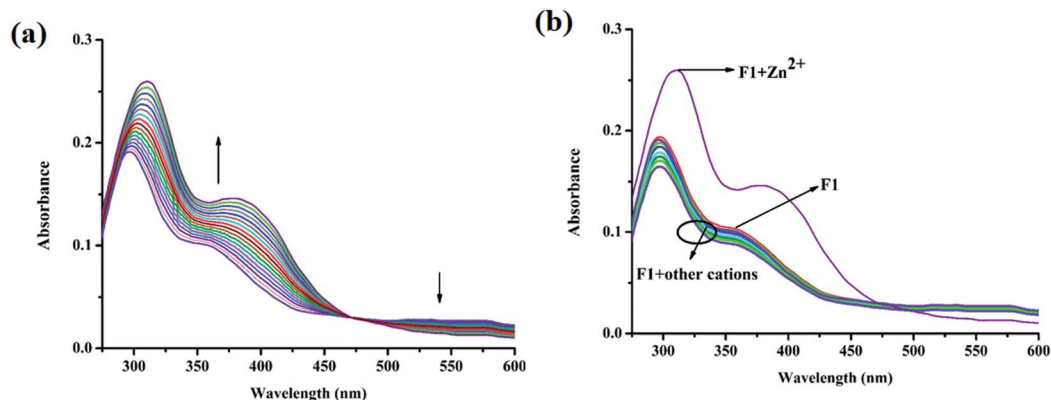Fig. 1 (a) The SC-XRD structure of **F1**. (b) The ChemDraw structure of **Z1**.

Fig. 2 (a) Changes in the absorption spectra of **F1** (20 μM) upon the gradual addition of Zn^{2+} (0–2000 μM) in HEPES-buffered EtOH/H_2O (4/1 v/v) media; pH: 7.4. (b) Absorption spectra of **F1** (20 μM) in the presence of different cations (2000 μM), *viz.* Zn^{2+}, K^+, Ca^{2+}, Mg^{2+}, Hg^{2+}, Pb^{2+}, Cr^{3+}, Mn^{2+}, Fe^{3+}, Co^{2+}, Ni^{2+}, Cu^{2+}, Zn^{2+}, Cd^{2+}, and Ag^+, in HEPES-buffered EtOH/H_2O (4/1 v/v) media; pH: 7.4.

Zn^{2+}, the absorbance increases along with the slight red-shifting of the peaks from 296 nm and 358 nm to 310 nm and 380 nm, respectively (Fig. 2a). The selectivity of **F1** towards Zn^{2+} is shown in Fig. 2b.

Also, the emission properties of **F1** were monitored *via* fluorescence spectroscopy. In the presence of Zn^{2+} the emission spectrum of **F1** is selectively perturbed, while other cations, *viz.* Al^{3+}, K^+, Ca^{2+}, Mg^{2+}, Hg^{2+}, Pb^{2+}, Cr^{3+}, Fe^{3+}, Mn^{2+}, Co^{2+}, Ni^{2+}, Cu^{2+}, Zn^{2+}, Cd^{2+} and Ag^+, have no effect (EtOH/H_2O: 4/1 v/v; 10 mM HEPES buffer; pH: 7.4; λ_{ex}: 332 nm; Fig. 3a). The weak emission of **F1** at 437 nm gradually increases to a 19-fold maximum upon the gradual addition of Zn^{2+} (Fig. 3b). Fluorescence behavior is susceptible to pH, and the Zn^{2+}-induced emission intensity of **F1** becomes highest at pH 7 (Fig. S4, ESI†). Hence, fluorescence experiments have been performed at physiological pH: 7.4. Competitive experiments indicate that there is no interference from common cations (Fig. S5, ESI†). Moreover, a sigmoidal plot of the emission intensity *vs.* [Zn^{2+}] has a linear region (Fig. S6, ESI†). The Zn^{2+} detection limit of **F1** is 42.23 nM (Fig. S7, ESI†). The binding constant calculated *via* the Benesi–Hildebrand equation is 7.71×10^4 M^{-1} (Fig. S8,

ESI†). The Job plot indicates a 1 : 3 (molar ratio) interaction between **F1** and Zn^{2+} (Fig. S9, ESI†).

Sensing mechanism

To obtain a plausible Zn(II) recognition mechanism in the presence of **F1**, a proper interpretation and understanding of
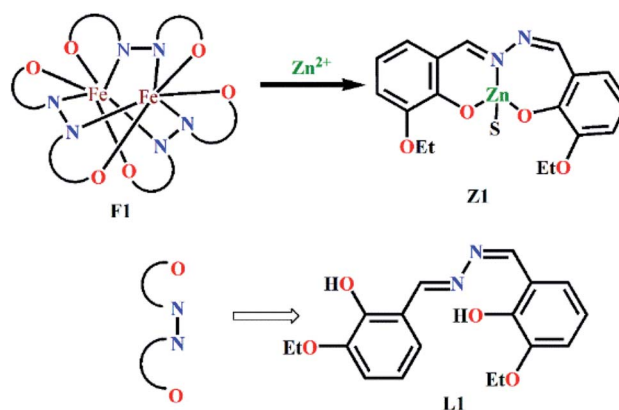
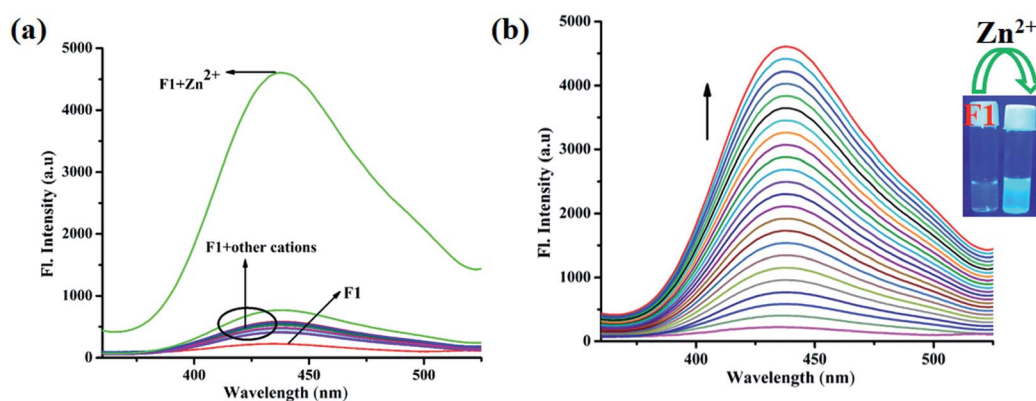**Scheme 2** A plausible fluorescence sensing mechanism.

Fig. 3 (a) Emission spectra of **F1** (20 μM) in the presence of different cations (2000 μM), *viz.* Zn^{2+}, K^+, Ca^{2+}, Mg^{2+}, Hg^{2+}, Pb^{2+}, Cr^{3+}, Mn^{2+}, Fe^{3+}, Co^{2+}, Ni^{2+}, Cu^{2+}, Zn^{2+}, Cd^{2+}, and Ag^+, in HEPES-buffered EtOH/H_2O (4/1 v/v) media; pH: 7.4; λ_{ex} = 332 nm. (b) Changes in the emission spectra of **F1** (20 μM) upon the gradual addition of Zn^{2+} (0–2000 μM) in HEPES-buffered EtOH/H_2O (4/1 v/v) media; pH: 7.4; λ_{ex} = 332 nm.
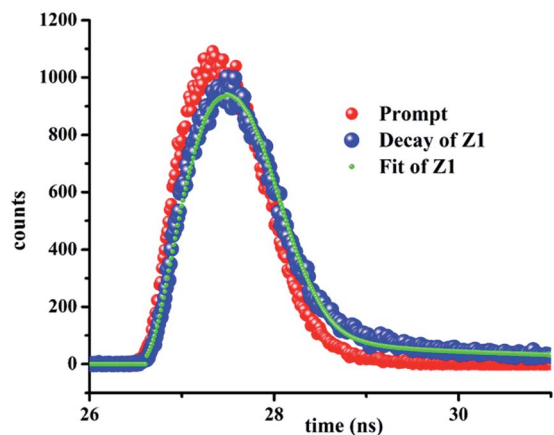
Fig. 4   The fluorescence lifetime decay profile of Z1 (F1 + Zn^{2+}).

Table 1   Fluorescence lifetime data of Z1

Sample	B_1	B_2	t_1 (ns)	t_2 (ns)	χ^2
Z1	78.82	22.18	0.23	3.25	0.96

the spectroscopic properties of F1 in the presence and absence of Zn(II) is very crucial. Thus, through interpreting the mass spectra, FTIR spectra and Job plot experiments, we can propose a "metal ion displacement protocol" as a plausible sensing mechanism (Scheme 2). The ν(N–N) band at 1140 cm^{-1} for F1 is shifted to 1227 cm^{-1} in the case of Z1. The absence of the ν(O–H) band in the case of Z1 also indicates the complexation of L1 with Zn^{2+}.

The selective recognition of an analyte by the probe using fluorescence spectroscopy is reflected by the fluorescence lifetime of the probe in the presence and absence of the analyte. Thus, Fig. 4 and Table 1 definitely suggest a significant interaction between F1 and Zn^{2+}, leading to fluorescence enhancement. Non-fluorescent F1 shows an average lifetime of 2.64 ns in the presence of Zn^{2+}.

It is very much expected that the two different systems possibly possess different morphologies, in terms of particle size, pattern, texture, etc. FESEM images indicate significant differences in morphological appearance between F1 and Z1 (Fig. 5). For F1, congested geometry is seen due to the large dinuclear Fe(III) complex, whereas changes detected in Z1, along
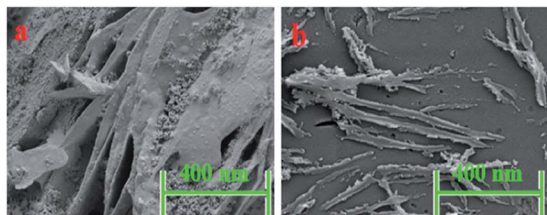

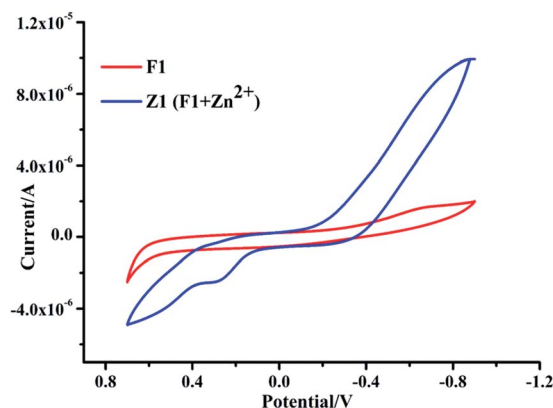Fig. 5   FESEM images of F1 (a) and Z1 (b).

Fig. 6   CV data from F1 and Z1.

with a reduction in particle size, reveal the formation of a mononuclear complex.

Furthermore, the electrochemical behaviours of the two different metal complexes seem to be different in terms of reversibility, redox potential, and $E_{1/2}$. Fig. 6 indicates that the electrochemical properties of Z1 are quite different from those of F1. The electrochemical behaviours of the F1 and [F1–Zn^{2+}] systems were monitored in anhydrous acetonitrile (ACN) media using tetra-butyl ammonium bromide (TBAB) as the supporting electrolyte at a scan rate of 100 mV s^{-1}, with [F1] = 1 × 10^{-4} M, [F1–Zn^{2+}] = 1 × 10^{-4} M, and [TBAB] = 0.1 M at room temperature. The redox process associated with F1 is quasi-reversible, having an $E_{1/2}$ value of +0.52 V, while the value is +0.31 V in the presence of Zn^{2+}. The cyclic voltammogram of F1 significantly differs in the presence of Zn^{2+}.

Kinetics of Fe(III) displacement from F1 by Zn^{2+}

The proposed mechanism of Fe(III) replacement from F1 by Zn(II) is kinetically followed via the stopped-flow technique, where the change in absorbance of F1 at 380 nm is monitored as a function of the amount of added Zn^{2+} ions. The Zn^{2+}-assisted absorbance enhancement is attributed to the displacement of Fe^{3+} by Zn^{2+} within ~1.2 s. The rate constant of the pseudo first-order displacement reaction with respect to Zn^{2+} is 2.7315 × 10^8 s^{-1} (Fig. S10, ESI†).

Extraction of Zn^{2+} using F1

F1 is also employed for the enrichment of Zn^{2+} via solvent extraction from water to ethyl acetate. Three organic solvents, viz. EtOAc, CHCl$_3$ and CCl$_4$, are tested for the extraction of Zn^{2+} from aqueous solution. F1 was equilibrated and partitioned at various concentrations (0.1 × 10^{-3}, 0.5 × 10^{-3}, 1.0 × 10^{-3}, 1.5
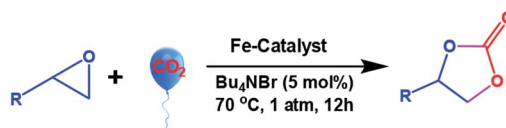
Scheme 3   The synthesis of cyclic carbonates from CO_2 and epoxides.
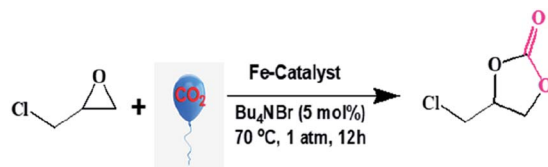
Scheme 4 The synthesis of a cyclic carbonate from CO_2 and epichlorohydrin.

$\times$ 10^{-3}, and 2.0×10^{-3} M) with known concentrations of Zn^{2+} for 1 h at room temperature. After the removal of the organic layer, the concentration of Zn^{2+} in the aqueous phase is measured using the presented method. The highest extraction efficiency is observed for EtOAc (95.47%), followed by chloroform (90.11%), and carbon tetrachloride (87.35%). The effects of various solvents on the extraction efficiency are presented in Fig. S11 (ESI).†

F1 catalyzed cyclic carbonate synthesis

The importance of the fixation of atmospheric CO_2 in the form of cyclic carbonates has already been discussed above. Hence, attempts have been made to study the catalytic activity of the new iron complex (**F1**) for the fixation of CO_2 as cyclic carbonates using different epoxides (Scheme 3).

The reaction of epichlorohydrin with CO_2 at 70 °C and under atmospheric pressure under solvent-free conditions, leading to a cyclic carbonate, is studied as a model reaction (Scheme 4). The reaction conditions have been optimized with respect to diverse parameters, *viz.*, temperature, reaction time and TBAB concentration, for maximum yield (Table S3, ESI†).

Among different trials, 5 mol% loading of co-catalyst (TBAB) led to the maximum yield of cyclic carbonate (Table S3, entry 9, ESI†). Above 5 mol% TBAB, no further improvement in product yield is observed. Traces of the desired product formed without

TBAB under identical reaction conditions. Interestingly, without the **F1** catalyst, TBAB alone fails to improve the yield of the product. A synergistic effect between **F1** and TBAB accelerated the product yield. It is noted that the reaction temperature plays a crucial role in determining the yield of the product (Table S3, ESI†). The highest yield is observed at 70 °C. Thus, the optimum parameters that lead to the highest yield of product are 5 mol% TBAB (co-catalyst), 70 °C (temp.), 12 h (reaction time), 15 mg of **F1** (catalyst load), and 1 atm. CO_2 (pressure) (Table S3, ESI†).

To verify the efficiency and performance of the **F1** catalyst, the fixation of CO_2 is tested with some substituted epoxides, like 1,2-epoxy-3-phenoxy propane epichlorohydrin and styrene oxide (Table 2). Of these, epichlorohydrin provided a better yield, probably due to the electron withdrawing effects of the substituent.

The catalytic efficiency of **F1**, the methodology, and the reaction conditions are highly competitive when compared with other reported iron catalysts (Table 3).

Plausible mechanism for epoxide formation

Based on experimental findings and the associated literature,[40–44] a plausible mechanism for fixing CO_2 using an epoxide, leading to an organic cyclic carbonate, is portrayed in Scheme 5. At first, the active site of **F1** coordinates with the O-donor of the epoxide, followed by nucleophilic attack by Br^- (from TBAB) at the C-centre attached to the epoxide oxygen; this opens the ring to form an α-halo-alkoxide. Then, the O-donor attached to the Fe centre interacts with the C-centre of CO_2 to produce an alkyl cyclic carbonate along with the regeneration of the catalyst **F1**.

Catecholase-like activity

The catecholase-like activity of **F1** (1×10^{-4} M) is monitored *via* time-dependent absorption spectroscopy through its reaction

Table 2 The synthesis of cyclic carbonates using the **F1** catalyst[a]

| Entry	Epoxide	Product	Yield[b] (%)	Conversion[c] (%)	TON[d]	TOF[e]
1			87	90	32 142	2678
2			97	99	35 357	2946
3			91	94	33 571	2797

[a] Reaction conditions: epoxide (5 mmol), **F1** catalyst (15 mg), TBAB (5 mol%), 70 °C, CO_2 (1 atm.), 12 h. [b] GC yield of cyclic carbonate. [c] Conversion is determined *via* GC. [d] Turnover number (TON) = (% conversion × mmol of substrate used)/(mmol of catalyst used). [e] Turnover frequency (TOF) = TON/time of reaction (h).

Table 3 Comparison of **F1** with some reported iron catalysts

Reaction	Catalyst	Reaction conditions	Yield (%)	Ref.
Cyclic carbonate synthesis	Iron(III)aminobis(phenolate) complexes	Epichlorohydrin (5.0×10^{-2} mol), PPNCl (5.00×10^{-5} mol), CO_2 (20 bar), 4 h, 100 °C	99	40
	Pyridine-bridged bispincer-type Fe(II) complex	Epichlorohydrin (10 mmol), TBAB (97.6 mg, 0.29 mmol), 25 °C, 0.5 MPa CO_2, 24 h.	91	41
	Fe(III) thio ether–triphenolate complex	Epichlorohydrin (7.0×10^{-2} mol), TBAB (7.0×10^{-5} mol), CO_2 (2 MPa); 100 °C, 6 h.	78	42
	F1	Epichlorohydrin (5 mmol), TBAB (5 mol%), 70 °C, CO_2 (1 atm.), 12 h	97	Present study

with the model compound 3,5-DTBC (1×10^{-2} M, 100 equiv.) in methanol under aerobic conditions at room temperature.

As saturation kinetics are observed at a high substrate concentration, the Michaelis–Menten equation and a Lineweaver–Burk plot (Fig. S12a, ESI†) are used to elucidate the kinetic parameters. The initial first order rate constant, V (s^{-1}), is calculated from the slope of the plot $\log[A_\infty/(A_{\infty\alpha} - A_t)]$ vs. time. Kinetic parameters like binding constant (K_M), maximum velocity (V_{max}), and rate constant (turnover number, k_{cat}) are determined from the linear plot of $1/V$ vs. $1/[S]$ (Lineweaver–Burk plot) as per the Michaelis–Menten enzymatic kinetics approach. From the Lineweaver–Burk plot, $1/V = \{K_M/V_{max}\} \times \{1/[S]\} + 1/V_{max}$, and the values for V_{max}, k_M, and k_{cat} are found to be 5.49×10^{-2} M s^{-1}, 1.23×10^{-4} M, and 4.42×10^3 h^{-1}.
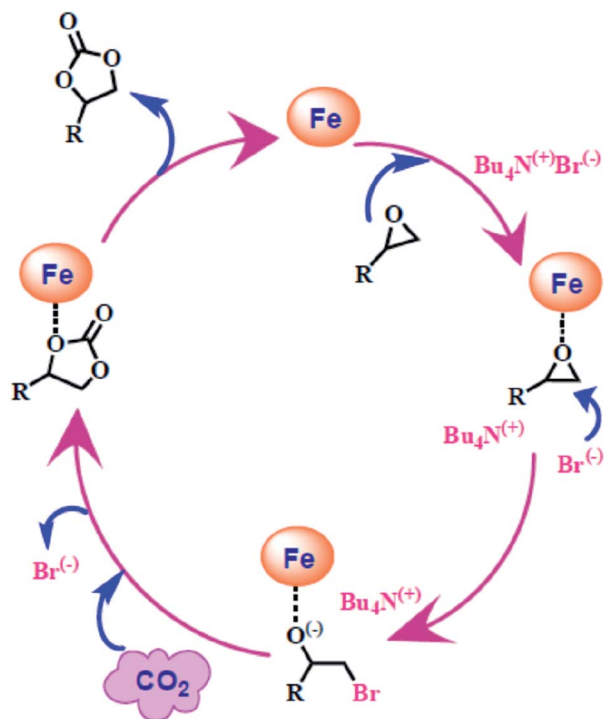
Scheme 5 The probable mechanistic pathway to organic cyclic carbonate formation.

Scheme S1 (ESI†) shows the well-known catalytic catechol oxidation protocol, supported by the ESI-MS(+) spectrum of a mixture of **F1** and 3,5-DTBC (1 : 50 molar ratio) in aqueous methanol (Fig. S12b, ESI†). The two predominant peaks at m/z values of 237.19 (calcd: 238.16) and 1135.13 (calcd: 1135.29) are attributed to $[3,5\text{-DTBQ} + H_2O]^+$ and $[\textbf{F1} + 2H_2O + Li]^+$, respectively.

The electrochemical transformation of catechol to quinone has also been monitored in the presence of **F1** (Fig. S12c, ESI†). The electrochemical behaviours of the **F1** and [**F1**-catechol] systems have been investigated in anhydrous acetonitrile media in the presence of tetra-butyl ammonium bromide (TBAB) as a supporting electrolyte at a scan rate of 100 mV s^{-1}, where [**F1**] $= 1 \times 10^{-4}$ M, [**F1**-catechol] $= 1 \times 10^{-4}$ M, and [TBAB] $= 0.1$ M, at room temperature. Cyclic voltammograms (CV) of the **F1** and [**F1**-catechol] systems appear different, with associated $E_{1/2}$ values of +0.52 V and +0.47 V, respectively.

Conclusion

A new dinuclear Fe(III) complex (**F1**) of a symmetrical azine derivative, structurally characterized via single-crystal X-ray analysis, is employed as a catalyst for the fixation of atmospheric CO_2 using epoxides, leading to organic cyclic carbonates with 97% yield. In addition, **F1** selectively recognizes Zn^{2+} at concentrations as low as 42.23 nM through TURN-ON fluorescence via a metal displacement protocol. Moreover, **F1** efficiently (95.47%) extracts Zn^{2+} from aqueous media to ethyl acetate. The catecholase-like activity of **F1** is demonstrated, providing a k_{cat} value of 4.42×10^3 h^{-1}.

Conflicts of interest

There are no conflicts to declare.

Acknowledgements

References

1 O. Ardon, H. Weizman, J. Libman, A. Shanzer, Y. Chen and Y. Hadar, *Microbiology*, 1997, **143**, 3625–3631.

2 A. Correa, O. Garca ̧ãanceÇoa and C. Bolm, *Chem. Soc. Rev.*, 2008, **37**, 1108–1117.

3 T. L. Foley and A. Simeonov, *Expet Opin. Drug Discov.*, 2012, **7**, 831–847.

4 L. Salmon, P. Thuery, E. Riviere and M. Ephritikhine, *Inorg. Chem.*, 2006, **45**, 83–93.

5 M. Graham, M. N. J. Paley, R. A. Grünewald and N. Hoggard, *Brain*, 2000, **123**, 2423–2431.

6 *CDC Breastfeeding Report Card, United states: Outcome Indicators (Publication, from Centers for Disease Control and Prevention*, National Immunization Survey, last accessed on, 11 May 2010.

7 J. M. Berg and Y. Shi, *Science*, 1996, **271**, 1081–1085.

8 N. P. Pavletich and C. O. Pabo, *Science*, 1991, **252**, 809–817.

9 C. O. Pabo and R. T. Sauer, *Annu. Rev. Biochem.*, 1992, **61**, 1053–1095.

10 K. A. McCall, C. C. Huang and C. A. Fierke, *J. Nutr.*, 2000, **130**, 1437S–1446S.

11 L. Vallee and K. H. Falchuk, *Phys. Rev.*, 1993, **73**, 79–118.

12 J. Y. Liang, Y. Y. Liu, J. Zou, R. B. Franklin, L. C. Costello and P. Feng, *Prostate*, 1999, **40**, 200–207.

13 K. Jobe, C. H. Brennan, M. Motevalli, S. M. Goldup and M. Watkinson, *Chem. Commun.*, 2011, **37**, 6036–6038.

14 S. Khanra, S. Ta, M. Ghosh, S. Chatterjee and D. Das, *RSC Adv.*, 2019, **9**, 21302–213010.

15 D. A. Pearce, N. Jotterand, I. S. Carrico and B. Imperiali, *J. Am. Chem. Soc.*, 2001, **123**, 5160–5161.

16 D. J. Darensbourg, *Inorg. Chem.*, 2010, **49**, 10765–10780.

17 M. Cokoja, C. Bruckmeier, B. Rieger, W. A. Herrmann and F. E. Kühn, *Angew. Chem., Int. Ed.*, 2011, **50**, 8510–8537.

18 M. Aresta, A. Dibenedetto and A. Angelini, *Chem. Rev.*, 2013, **114**, 1709–1742.

19 R. Li, X. Tong, X. Li and C. Hu, *Pure Appl. Chem.*, 2012, **84**, 621–636.

20 N. Kielland, C. J. Whiteoak and A. W. Kleij, *Adv. Synth. Catal.*, 2013, **355**, 2115–2138.

21 M. North, R. Pasquale and C. Young, *Green Chem.*, 2010, **12**, 1514–1539.

22 J. H. Clements, *Ind. Eng. Chem. Res.*, 2003, **42**, 663–674.

23 K. Motokura, S. Itagaki, Y. Iwasawa, A. Miyaji and T. Baba, *Green Chem.*, 2009, **11**, 1876–1880.

24 E. A. Prasetyanto, M. B. Ansari, B.-H. Min and S.-E. Park, *Catal. Today*, 2010, **158**, 252–257.

25 H. Zhou, Y.-M. Wang, W.-Z. Zhang, J.-P. Qu and X. B. Lu, *Green Chem.*, 2011, **13**, 644–650.

26 I. Bauer and H. J. Knölker, *Chem. Rev.*, 2015, **115**, 3170–3387.

27 A. Buchard, M. R. Kember, K. G. Sandeman and C. K. Williams, *Chem. Commun.*, 2011, **47**, 212–214.

28 C. J. Whiteoak, E. Martin, M. M. Belmonte, J. BenetBuchholz and A. W. Kleij, *Adv. Synth. Catal.*, 2012, **354**, 469–476.

29 K. S. Banu, T. Chattopadhyay, A. Banerjee, S. Bhattacharya, E. Suresh, M. Nethaji, E. Zangrando and D. Das, *Inorg. Chem.*, 2008, **47**, 7083–7093.

30 S. Majumder, S. Sarkar, S. Sasmal, E. Carolina Sãnudo and S. S. Mohanta, *Inorg. Chem.*, 2011, **50**, 7540–7554.

31 A. Biswas, L. K. Das, M. G. B. Drew, C. Diaz and A. Ghosh, *Inorg. Chem.*, 2012, **51**, 10111–10121.

32 A. Neves, L. M. Rossi, A. J. Bortoluzzi, B. Szpoganicz, C. Wiezbicki and E. Schwingel, *Inorg. Chem.*, 2002, **41**, 1788–1794.

33 P. Comba, B. Martin, A. Muruganantham and J. Straub, *Inorg. Chem.*, 2012, **51**, 9214–9225.

34 M. Mitra, A. K. Maji, B. K. Ghosh, G. Kaur, A. R. Choudhury, C.-H. Lin, J. Ribas and R. Ghosh, *Polyhedron*, 2013, **61**, 15–19.

35 J. Wang, W. Lin and W. Li, *Chem.–Eur. J.*, 2012, **18**, 13629–13632.

36 L. H. Feng, C. L. Zhu, H. X. Yuan, L. B. Liu, F. T. Lv and S. Wang, *Chem. Soc. Rev.*, 2013, **42**, 6620–6633.

37 G. B. Li, H. C. Fang, Y. P. Cai, Z.-Y. Zhou, P. K. Thallapally and J. Tian, *Inorg. Chem.*, 2010, **49**, 7241.

38 M. Ghosh, S. Ta, M. Banerjee and D. Das, *ACS Omega*, 2018, **3**, 16089–16098.

39 O. V. Dolomanov, L. J. Bourhis, R. J. Gildea, J. A. K. Howard and H. Puschmann, *J. Appl. Crystallogr.*, 2009, **42**, 339–341.

40 Y. Ge, G. Cheng, N. Xu, W. Wang and H. Ke, *Catal. Sci. Technol.*, 2019, **9**, 4255–4261.

41 H. Ullah, B. Mousavi, H. A. Younus, Z. A. K. Khattak, S. Suleman, M. T. Jan, B. Yu, S. Chaemchuen and F. Verpoort, *J. Catal.*, 2019, **377**, 190–198.

42 Z. A. K. Khattak, H. A. Younus, N. Ahmad, H. Ullah, S. Suleman, M. S. Hossain, M. Elkadi and F. Verpoort, *Chem. Commun.*, 2019, **55**, 8274–8277.

43 F. Chen, N. Liu and B. Dai, *ACS Sustainable Chem. Eng.*, 2017, **5**, 9065–9075.

44 A. Buonerba, A. De Nisi, A. Grassi, S. Milione, C. Capacchione, S. Vagin and B. Rieger, *Catal. Sci. Technol.*, 2015, **5**, 118–123.